Progress In Electromagnetics Research M, Vol. 74, 115–123, 2018

Research on Torque Ripple Optimization of Switched Reluctance Motor Based on Finite Element Method

Libing Jing* **and Jia Cheng**

Abstract—Torque ripple is the main cause of motor vibration and noise. In order to reduce the torque ripple of the switched reluctance motor (SRM), a new type of rotor tooth profile is studied, namely adding a semi-oval auxiliary core on both sides of the conventional parallel rotor tooth profile. Using a finite element method, a 12/8-pole SRM was modeled, and an optimal modified model was obtained through parameterized simulation. At the same time, in order to further reduce the torque ripple, the turn-on and turn-off angles of the power converter are optimized, and the torque jump caused by the commutation phase is alleviated. The combination of turn-on and turn-off angles is obtained through simulation calculation, and it can not only significantly reduce the torque ripple of the SRM, but also alleviate the local saturation caused by the double salient pole. This method can reduce the local saturation caused by the double salient structure and the large torque jump caused by the commutation phase. This method is of reference for other double salient motors.

1. INTRODUCTION

Switched reluctance motor has no rotor windings and permanent magnets. Therefore, it has a simple structure, low cost and high reliability. It is suitable for harsh environments such as high speed and high temperature. SRM has always been regarded as one of the best solutions for electric vehicle drive systems [1, 2]. However, the vibration and noise caused by torque ripple has been the main bottleneck limiting the universal application of the SRM. Therefore, minimizing the torque ripple of a SRM has become one of the hot issues of many SRM researchers today.

There are three main reasons for the torque ripple generated by a SRM: (1) edge flux; (2) local saturation of the exciter magnetic poles and the rotor pole due to the double salient pole structure; (3) The phase current and torque jump are caused by switching power converter circuit in switched reluctance motor system [3, 4]. These three aspects lead to inherent torque ripple of the SRM domestic and foreign scholars mainly reduce the torque ripple of SRM by optimizing the structure and control strategy of the motor. However, most of the literature research focuses on the field of control. Many scholars proposed new intelligent control strategies based on the torque distribution control strategy [5], variable structure control strategy [6], and modern control theory [7, 8]. The method of control field increases the complexity of the controller and cost of the motor. Therefore, the research on reducing the torque ripple of the SRM through the design of the motor body structure has gained attention in recent years.

In [9–11], an SRM body structure is taken as the research object, and the influence of the opening position and opening size of the rotor core on the torque ripple is analyzed. This method reduces the torque ripple of the motor by changing the magnetic field distribution inside the rotor. In [12, 13], in order to reduce the torque ripple of SRM, a V-shaped slot of appropriate size is opened on the side of each rotor pole, and the opening of the V-shaped slot faces the direction of rotation. However,

Received 11 July 2018, Accepted 21 September 2018, Scheduled 11 October 2018
* Corresponding author: Libing Jing (jinglibing163@163.com).
The authors are with the College of Electrical Engineering & New Energy, China Three Gorges University, Yichang 443002, China.

the shortcoming of this method is that the torque ripple can only be reduced in one direction, and the average torque is reduced. In [14, 15], the influence of the edge flux is improved by changing the SRM stator and rotor pole piece structure, thereby reducing the motor torque ripple. The effects of four different rotor tooth profiles on torque ripple were compared by Maxwell tensor method [16]. In [17–20], the air gap magnetic density is improved based on changing the stator pole surface structure to form an uneven air gap, thereby reducing the SRM torque ripple. However, there is little research on the local saturation of the exciter magnetic poles and the rotor pole due to the double salient pole structure.

In order to reduce the SRM torque ripple, a new rotor tooth profile is studied. On the basis of the parallel teeth of the conventional SRM, a semi-elliptical auxiliary iron core is added on both sides of the rotor magnetic pole, and the conventional rotor parallel teeth are changed into a drum type tooth structure. The added semi-elliptical core long axis is fixed to the rotor pole length, and the ratio of the short axis to the long axis of the semi-elliptical core is defined as the coefficient P. The torque ripple of the SRM is reduced by optimizing the coefficient P. Therefore, an improved model of the SRM is obtained. In order to further reduce the torque of the SRM, the effects of turn-on and turn-off angles on the torque ripple are studied. By optimizing the turn-on angle and the turn-off angle, the optimized model of the switched reluctance motor is obtained, and the torque ripple is significantly reduced.

2. TORQUE RIPPLE OPTIMIZATION DESIGN

The design scheme is proposed by the source generated by the torque ripple of the SRM. In order to alleviate the local saturation of the exciter magnetic poles and the rotor pole caused by the double salient pole structure, a new type of SRM rotor tooth profile is studied. A semi-elliptical auxiliary iron core is added on both sides of the parallel teeth of the conventional SRM. As shown in Fig. 1 the semi-elliptical auxiliary core long axis h_r is fixed to the rotor pole length, and d represents the semi-short axis distance. The ratio of the short axis to the long axis of the auxiliary core is defined as the coefficient P:

$$P = \frac{2d}{h_r} \tag{1}$$

The variable d is set in the finite element software. Through the comparison of the parametric simulation results, the optimal semi-short axis distance d is found, and the optimal coefficient P is calculated. The improved model of SRM motor is obtained.

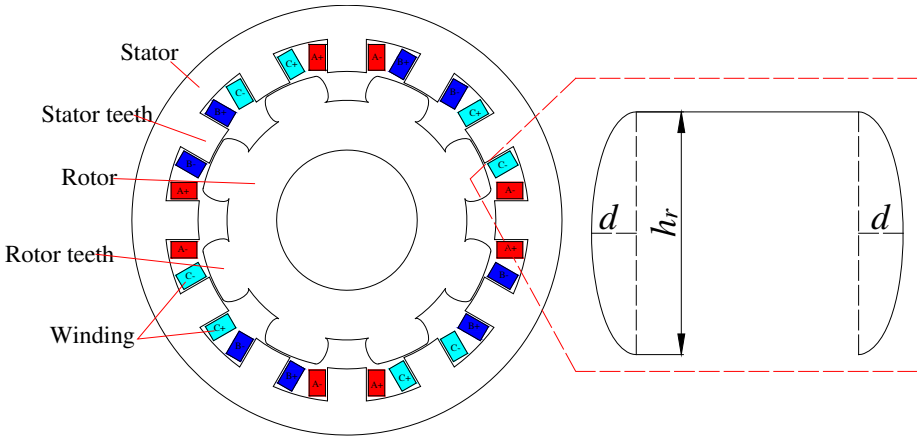

Figure 1. Improved SRM model.

In order to alleviate the transition of phase current and torque, the optimal combination of opening angle and turn-off angle is obtained by optimizing the opening angle and the turn-off angle of the power converter. By optimizing the turn-on angle and turn-off angle, finding the optimal opening angle and closing angle combination scheme, the optimized model of the switched reluctance motor is obtained.

3. MODEL OF SRM

This paper takes the rated power 15 kW, rated voltage 220 V, rated speed 1500 r/min, three-phase 12/8 pole SRM as an example. The finite element software Ansoft Maxwell was used to establish a two-dimensional field-circuit coupling model to study the influence of motor torque ripple. The main parameters of the motor are shown in Table 1.

Table 1. Main parameters of motor structure.

Parameter	value	Parameter	value
Stator pole number	12	Rotor pole number	8
Stator outer diameter/mm	260	Rotor outer diameter/mm	178
Stator inner diameter/mm	180	Rotor inner diameter/mm	85
Stator yoke height/mm	20	Rotor yoke height/mm	30
Stator pole arc/(°)	15	Rotor pole arc/(°)	16
Air gap length/mm	1	Iron core length/mm	200

4. CALCULATION RESULTS AND ANALYSIS

The torque ripple factor K_T is defined as:

$$K_T = \frac{T_{\max} - T_{\min}}{T_{av}} \times 100\% \tag{2}$$

where $T_{\max}$ is the maximum torque value when the motor is running stably, $T_{\min}$ the minimum torque value when the motor is running stably, and T_{av} the average torque value when the motor is running stably.

4.1. Transient Magnetic Field Analysis

The simulation results of the motor are shown in Fig. 2. Compared with the conventional SRM structure, the motor flux path saturation is greatly reduced after the motor adopts the new rotor tooth profile.

In order to reduce the local saturation when the stator poles are aligned, a semi-elliptical core is added on both sides of the rotor of the conventional SRM, and the long axis is fixed to the rotor pole length. By changing the coefficient P, the torque ripple result is calculated as shown in Fig. 3.

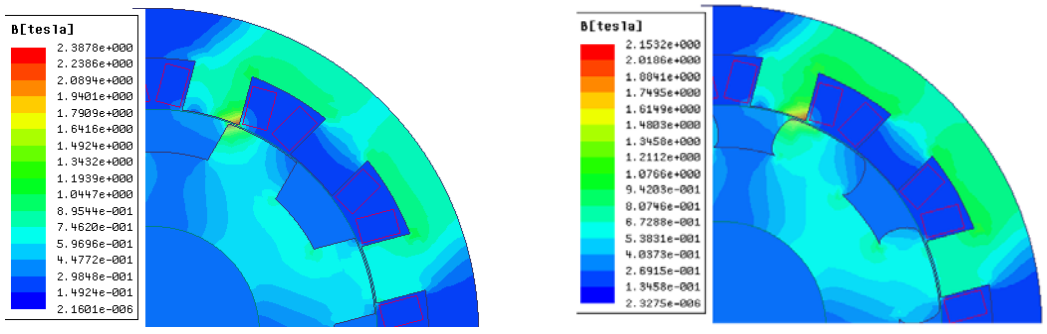

(a) (b)

Figure 2. Magnetic field distribution. (a) Conventional model. (b) Improved model.

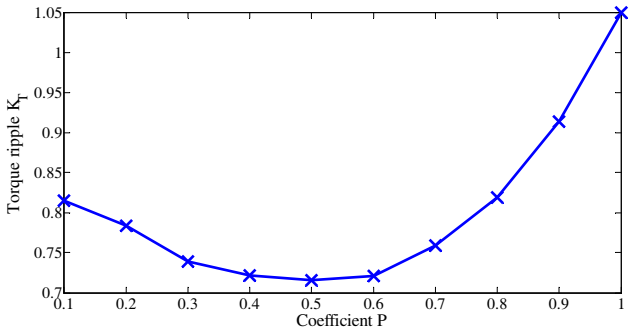

Figure 3. The influence of coefficient P on torque ripple.

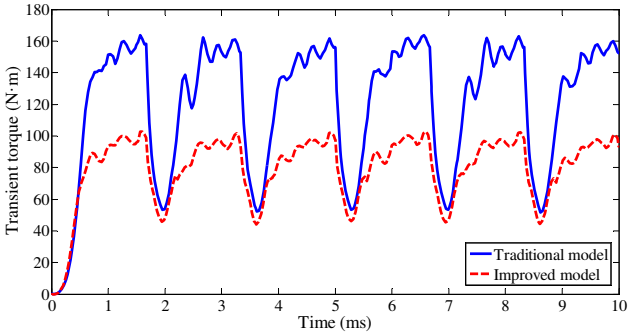

Figure 4. Comparison diagram of instantaneous torque.

As shown in Fig. 3, as the coefficient P increases, the semi-short axis d of the auxiliary core increases, and the torque ripple coefficient of the SRM decreases. When the coefficient P exceeds 0.6, the torque ripple coefficient increases sharply. In general, torque ripple coefficient decreases first and then increases. The torque ripple was the minimum within the range of 0.4–0.6.

The calculation results are shown in Table 2: coefficient P is in the range of 0.4–0.6, and the torque ripple is the smallest. In order to further accurately reduce the torque ripple coefficient of the SRM, the parameterized simulation step size is reduced. It can be seen from the calculation results that when coefficient P is 0.46, the torque ripple coefficient is at least 70.27%.

Table 2. The influence of coefficient P on torque ripple.

Coefficient P	Torque ripple coefficient K_T
0.4	72.15%
0.5	71.58%
0.6	72.09%

According to the previous simulation calculation, when coefficient P is 0.46, the torque ripple coefficient is the smallest, and an improved model of the switched reluctance motor is obtained. A comparison chart of the transient torque waveforms of the improved SRM model compared to the conventional SRM model is shown in Fig. 4.

As shown in Fig. 4, the motor speed is 1500 r/min, and a simulation cycle time is taken as 10 ms to obtain the transient torque waveform of the motor starting to steady state. It can be seen from Fig. 4 that the torque ripple coefficient of the improved model switched reluctance motor is significantly reduced. This improved method has a peak clipping effect, and the torque ripple is significantly reduced. After calculation, the torque ripple coefficient of the conventional motor model is 90.37%; the average torque is 127.35 N · m; the improved model motor torque ripple coefficient obtained by adding a semi-elliptical auxiliary iron core on both sides is 70.27%; the average torque is 83.57 N · m. It can be seen from the calculation results that compared with the conventional motor model, the improved motor model torque ripple coefficient decreases by 22.24%, and the average torque decreases by 34.37%.

Take a point on the rotor magnetic pole and simulate the magnetic density waveform curve with time. The comparison diagram of magnetic density at a certain point of rotor between the conventional model and improved model is shown in Fig. 5.

As can be seen from Fig. 5, the maximum magnetic density of the rotor pole of the conventional model is 2.13 T, and the maximum value of the improved model is 1.85 T, which is 13.15% lower than the conventional model. It can be seen from the magnetic density comparison diagram that the new rotor tooth profile model can reduce the local saturation of the exciter magnetic poles and rotor pole,

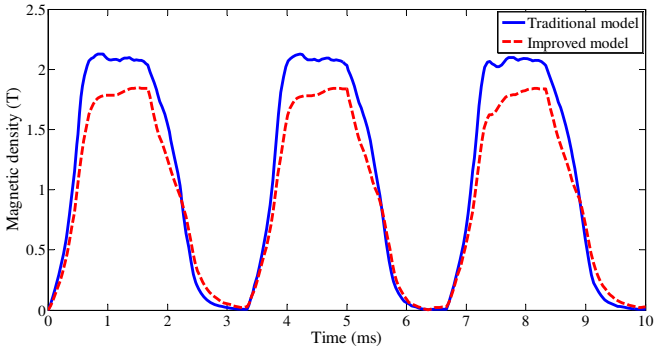

Figure 5. Comparison diagram of magnetic density.

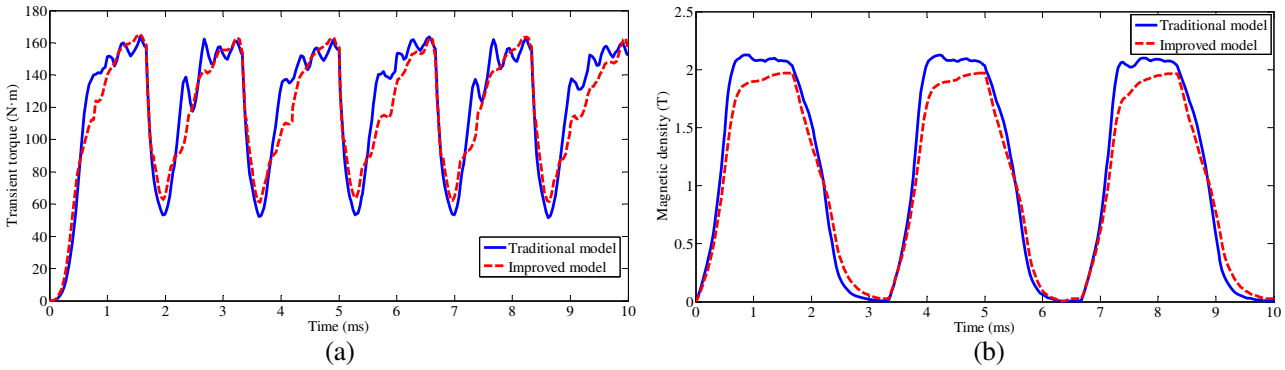

Figure 6. Comparison diagram of instantaneous torque and magnetic density. (a) Comparison diagram of instantaneous torque. (b) Comparison diagram of magnetic density.

and verify the correctness of the model.

However, compared with the conventional model, the average output torque is reduced. To overcome this disadvantage, the method of increasing the current can be used to increase the output torque. As shown in Fig. 6, when the current is increased by 1.11 times, the conventional model and improved model of the SRM instantaneous torque comparison diagram and the magnetic density comparison diagram are obtained.

As can be seen from Fig. 6(a), the torque ripple factor is still reduced compared to the conventional model. After calculation, when the current increases by 1.11 times, the improved model torque ripple coefficient is 82.53%, which is 8.68% lower than the traditional model. It can be seen from Fig. 6(b) that when the current is increased by 1.11 times, the maximum value of the improved model rotor magnetic density is 1.97 T, which is 7.5% lower than that of the conventional model. The simulation results further verify the effectiveness of the design. The improved model can effectively alleviate the local saturation of the exciter magnetic poles and the rotor pole caused by the double salient pole structure, and can reduce the torque ripple of the switched reluctance motor.

4.2. Static Magnetic Field Analysis

For the static magnetic field analysis of SRM, the current source is used as the excitation, and the single-phase winding excitation method is used for analysis. The stator winding current is 20 A. The simulation period is that the rotor of the motor rotates at a rotor pole angle of 45°. The static torque comparison diagram between the conventional model and improved model is obtained by finite element software simulation, as shown in Fig. 7.

It can be seen from Fig. 7 that the static maximum torque of the conventional model is 161.25 N · m, and the static maximum torque of the new model with the addition of the auxiliary core is 143.63 N · m,

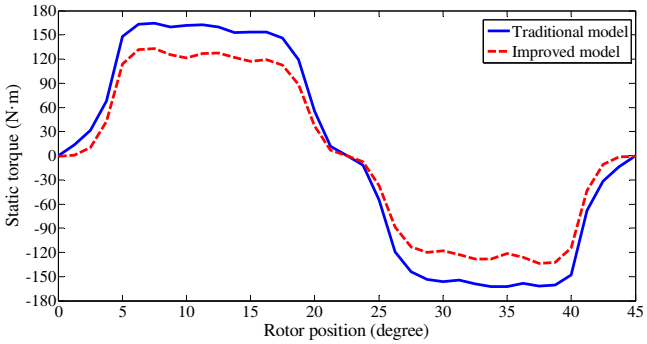

Figure 7. Comparison diagram of static torque between conventional model and improved model.

which is 10.93% lower than the conventional model. By adding an auxiliary iron core on both sides of the rotor tooth, the local saturation of the exciter magnetic poles and the rotor pole caused by the double salient pole structure is alleviated, thereby miniaturizing the peak of torque and reducing the torque ripple of SRM.

4.3. Influence of Turn-on Angle and Turn-off Angle on Torque Ripple

In order to alleviate the phase current and torque jump caused by the switch-type power converter circuit of the SRM, the optimal switching on and off angles combination scheme is found by optimizing the turn-on angle and turn-off angle. The conventional SRM adopts a combination scheme of turn-on angle 0° and turn-off angle 15° [3]. As shown in Fig. 8, the motor speed is 1500 r/min; the A phase closing time is 1.6670 ms; the corresponding turn-off angle is 15°. At this time, the phase A current is attenuating; the B phase is just turned on; the current is increasing. At the moment of commutation, the phase A torque starts to decrease from the maximum value; the phase B torque rises from zero; the output torque is the superposition of the phase A torque and the phase B torque, thus causing a torque jump and large torque ripple.

In order to minimize the torque jump caused by the commutation time, the effect of the turn-off angle on the torque ripple is studied by using the scheme of the turn-off angle hysteresis. The calculation results are shown in Fig. 9.

As shown in Fig. 9, as the turn-off angle increases, the torque ripple coefficient of the SRM decreases significantly. However, when the turn-off angle is too large, the torque ripple coefficient increases instead. When the turn-off angle is 18°, the torque ripple coefficient of the improved SRM model is the smallest, which is 0.3041, and the torque ripple coefficient is reduced by 56.72% compared with the conventional solution turn-off angle of 15°.

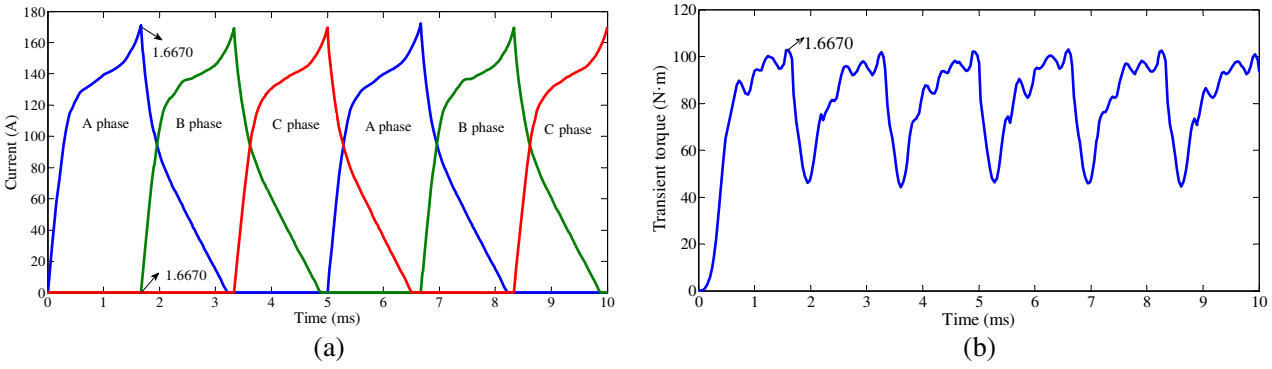

Figure 8. Improved model under conventional switching on and off angles scheme. (a) Current waveform. (b) Transient torque waveform.

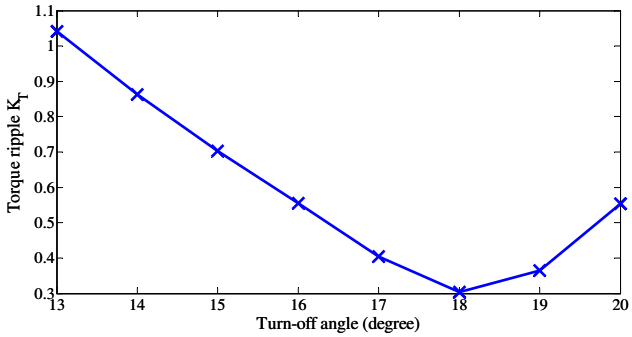

Figure 9. The effect of turn-off angle on torque ripple.

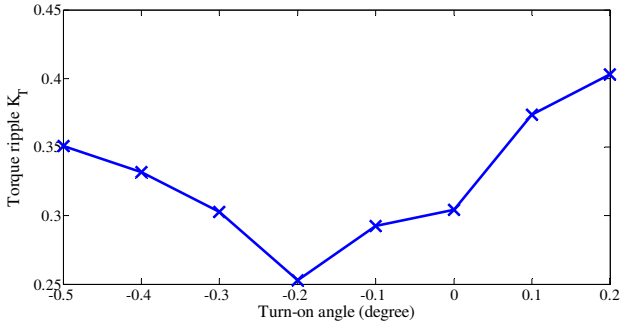

Figure 10. The effect of turn-on angles on torque ripple.

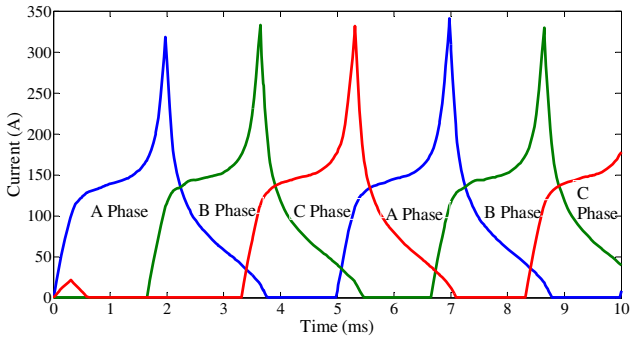

Figure 11. Current waveform after switching on and off optimization.

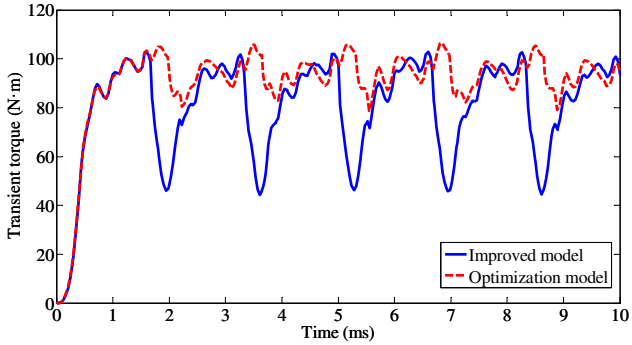

Figure 12. Comparison diagram of instantaneous torque.

In order to further reduce the torque ripple coefficient of the SRM, the turn-off angle is fixed to 18°, and the influence of the turn-on angle on the torque ripple coefficient is studied. The calculation result is shown in Fig. 10.

After the turn-off angle is fixed at 18°, the turn-on angle is fine-tuned. As shown in Fig. 10, as the turn-on angle increases, the torque ripple coefficient of the SRM decreases first and then increases. When the turn-on angle is −0.2°, that is, compared with the conventional turn-on angle, the ABC phases are turned on 0.2° ahead of time, and the torque ripple coefficient is at least 0.2528.

In summary, in order to alleviate the torque change at the commutation time, a combination of a turn-on angle of −0.2° and turn-off angle of 18° is adopted, and the torque ripple of the SRM is the smallest. Compared with the conventional solution turn-on angle of 0° and the turn-off angle of 15°, the torque ripple coefficient is reduced by 64.02%. The current waveform after the turn-on angle and turn-off angle optimization scheme is shown in Fig. 11.

It can be seen from Fig. 11 that when phase B current is turned on, phase A current is not turned off, which reduces the torque ripple caused by the commutation. The instantaneous torque comparison diagram of the improved model and optimized model of the switched reluctance motor is shown in Fig. 12.

As shown in Fig. 12, on the basis of the improved model, after the optimization of the turn-on angle and turn-off angle, the torque jump is significantly reduced at the moment of commutation. Compared with the improved model, not only the optimized SRM model torque ripple coefficient is significantly reduced, but also the average output torque is significantly increased. However, compared with the conventional model, the output torque is still reduced, which can be compensated by increasing the current. The effects of the three models on the torque ripple coefficient and average output torque of the switched reluctance motor are shown in Table 3.

Table 3. Torque ripple effect under three models.

Types	Torque ripple coefficient K_T	Average output torque ($\mathrm{N}\cdot\mathrm{m}$)
Conventional model	90.37%	127.35
Improved model	70.27%	83.57
Optimization model	25.28%	95.69
Final effect	Decrease 72.03%	Decrease 24.94%

5. CONCLUSION

(1) Considering the SRM electromagnetic characteristics, edge flux and other factors, the auxiliary elliptical core is added to both sides of the conventional SRM parallel rotor tooth profile from the structure design of the motor body, and the 12/8 pole motor simulation model is constructed. The electromechanical dynamic response characteristics of the motor magnetic field, torque ripple and other transient processes are simulated, and the relationship between the ratio of the minor axis to the long axis of the auxiliary core and the torque ripple is verified. The torque ripple coefficient is significantly reduced by selecting the appropriate coefficient.

(2) The combination of the optimized turn-on angle and turn-off angle can alleviate the torque jump caused by SRM commutation. From the simulation results, the optimized model mitigates the torque jump during commutation, resulting in a significant reduction in torque ripple coefficient. However, compared with the conventional model, the average output torque is reduced. To overcome this disadvantage, the method of increasing the current can be used to increase the output torque.

This method can reduce the torque ripple of SRM as well as the local saturation of the motor and can ease the commutation torque caused by the big jump; this method has reference significance for other doubly salient motors.

ACKNOWLEDGMENT

This work was supported by the National Natural Science Foundation of China (Project No. 51707072), China Postdoctoral Science Foundation (Project No. 2018M632855), and the thesis Foundation of China Three Gorges University (Project No. 2018SSPY079).

REFERENCES

1. Zhu, J., K. W. E. Cheng, and X. Xue, "Design of a new enhanced torque in-wheel switched reluctance motor with divided teeth for electric vehicles," *IEEE Trans. Magn.*, Vol. 53, No. 11, ID:2501504, Nov. 2017.
2. Cao, X., J. Zhou, and C. Liu, "Advanced control method for single-winding bearingless switched reluctance motor to reduce torque ripple and radial displacement," *IEEE Trans. Energy Convers.*, Vol. 32, No. 4, 1533–1543, Jun. 2017.
3. Lawrenson, P. J., J. M. Stephenson, and P. T. Blenkinsop, "Variable-speed switched reluctance motors," *Electric Power Applications IEE Proceedings B*, Vol. 127, No. 4, 253–265, Jul. 1980.
4. Li, Z., L. Zheng, and W. Yang, "Research on torque ripple and structure optimization of switched reluctance motor," *Electric Machines and Control.*, Vol. 22, No. 6, 11–21, Jul. 2018.
5. Yao, S. and W. Zhang, "A simple strategy for parameters identification of SRM direct instantaneous torque control," *IEEE Trans. on Power Electro.*, Vol. 33, No. 4, 3622–3630, Apr. 2018.
6. Rafiq, M., S. U. Rehman, and F. U. Rehman, "A second order sliding mode control design of a switched reluctance motor using super twisting algorithm," *Simulation Modelling Practice & Theory*, Vol. 25, No. 6, 106–117, Jun. 2012.

7. Ye, W., Q. Ma, and P. Zhang, "Torque ripple reduction in switched reluctance motor using a novel torque sharing function," *2016 IEEE International Conference on Aircraft Utility Systems*, 177–182, 2016.
8. Cai, Y., S. Sun, and C. Wang, "The research on flux linkage characteristic based on BP and RBF neural network for switched reluctance motor," *Progress In Electromagnetics Research M*, Vol. 35, 151–161, 2014.
9. Samani, O. N. and B. Ganji, "Noise reduction of switched reluctance motors," *2017 8th Power Electronics, Drive Systems & Technologies Conference*, 300–304, 2017.
10. Sahin, C., A. E. Amac, and M. Karacor, "Reducing torque ripple of switched reluctance machines by relocation of rotor moulding clinches," *IET Electric Power Applications*, Vol. 6, No. 9, 753–760, Nov. 2012.
11. Faiz, J., F. Tahvilipour, and G. Shahgholian, "Performance improvement of a switched reluctance motor," *PIERS Proceedings*, Vol. 49, No. 1, 728–732, Kuala Lumpur, Malaysia, Mar. 27–30, 2012.
12. Jin, W. L., S. K. Hong, and B. I. Kwon, "New rotor shape design for minimum torque ripple of SRM using FEM," *IEEE Trans. Magn.*, Vol. 40, No. 2, 754–757, Mar. 2004.
13. Li, G., J. Ojeda, and S. Hlioui, "Modification in rotor pole geometry of mutually coupled switched reluctance machine for torque ripple mitigating," *IEEE Trans. Magn.*, Vol. 48, No. 6, 2025–2034, Jun. 2012.
14. Ozoglu, Y., M. Garip, and E. Mese, "New pole tip shapes mitigating torque ripple in short pitched and fully pitched switched reluctance motors," *Electric Power Systems Research*, Vol. 74, No. 1, 95–103, Dec. 2005.
15. Sundaram, M., P. Navaneethan, and M. Vasanthakumar, "Magnetic analysis and comparison of switched reluctance motors with different stator pole shapes using a 3D finite element method," *2009 International Conference on Control, Automation, Communication and Energy Conservation*, 1–4, 2009.
16. Cai, Y. and D. X. Zhang, "Simulation study on torque ripple reduction of a switched reluctance motor using new rotor tooth," *Transactions of China Electrotechnical Society*, Vol. 30, No. 2, 64–70, Dec. 2015.
17. Yong, K. C., H. S. Yoon, and S. K. Chang, "Pole-shape optimization of a switched-reluctance motor for torque ripple reduction," *IEEE Trans. Magn.*, Vol. 43, No. 4, 1797–1800, Apr. 2007.
18. Sheth, N. K. and K. R. Rajagopal, "Torque profiles of a switched reluctance motor having special pole face shapes and asymmetric stator poles," *IEEE Trans. Magn.*, Vol. 40, No. 4, 2035–2037, Aug. 2004.
19. Lee, J. H., E. W. Lee, and Y. C. Cho, "Characteristic analysis of single phase SRM with stepped rotor pole face by FEM," *2006 12th Biennial IEEE Conference on Electromagnetic Field Computation*, 153–153, 2006.
20. Torkaman, H. and S. E. Afjei, "Comparison of three novel types of two-phase switched reluctance motors using finite element method," *Progress In Electromagnetics Research*, Vol. 125, 151–164, 2012.